ECS Electrochemistry Letters, **2** (11) A111-A113 (2013)
2162-8726/2013/2(11)/A111/3/$31.00 © The Electrochemical Society

First Principles Prediction on the Formation and Properties of Polyanion Deficient Iron Phosphate

Yu-Hao Tsai,[a] Chia-Yun Chou,[a,*] Kyoung E. Kweon,[b] Sei-Ung Park,[c] Kyu-Ho Song,[c] Chang-Keun Back,[c] and Gyeong S. Hwang[a,b,,z]**

[a]*Materials Science and Engineering Program, The University of Texas at Austin, Austin, Texas 78712, USA*
[b]*Department of Chemical Engineering, The University of Texas at Austin, Austin, Texas 78712, USA*
[c]*Battery Materials Group, Hanwha Chemical R&D Center, Daejeon 305-804, Korea*

We evaluate the possible formation of recently proposed PO_4-deficient $FePO_4$ by calculating its structure and stability at various charge states using the DFT+U theory. Unpaired electrons resulting from PO_4 deficiency tend to localize on undercoordinated Fe neighbors. The absence of a PO_4 unit causes local lattice distortions which are found to be sensitive to the charge state. Our calculations show that neutral and negatively charged PO_4 vacancies may coexist under intrinsic conditions. The PO_4-deficient $FePO_4$ matrix turns out to be substantially softened, which may contribute to enhanced Li diffusion and provide clues toward the design of high performance $LiFePO_4$ cathode.
 [DOI: 10.1149/2.010311eel]

Manuscript submitted July 3, 2013; revised manuscript received August 15, 2013. Published September 5, 2013.

Lithium iron phosphate $LiFePO_4$ (LFP) has recently emerged as an attractive cathode material for next-generation lithium ion batteries (LIBs) because of its remarkable thermal and chemical stability, nontoxicity, low cost, and reasonably high theoretical capacity ($\approx$ 170 mAh/g).[1,2] However, the practical use of LFP is hampered by its intrinsically poor electrical and ionic conductivities.[3,4] Considerable efforts have been made to overcome these drawbacks, including heterogeneous doping and defect engineering. For instance, aliovalent doping with Nb, Mg, Zr and Ti has been demonstrated to enhance the LFP electrical conductivity by eight orders of magnitude up to about 10^{-2} S/cm[5] (which is comparable to that of the most commonly used $LiCoO_2$ and $LiMn_2O_4$).[6] In addition, proper control of native defects (such as Li vacancies/interstitials) and Li-Fe ion exchanging antisite defects was also suggested to have positive impacts on Li mobility enhancement.[7–9] While the underlying mechanisms still remain a controversial topic, above findings seed the idea of enhancing the electronic and ionic conduction simultaneously in LFP via structural modifications at the atomic level. Very recently, a viable synthesis method was proposed to control the polyanion deficiency in a lithiated metal phosphate matrix,[10] but the atomic details have not been explored. In this letter, we present the structure and properties of phosphate (PO_4)-deficient $FePO_4$ based on density functional theory (DFT) calculations.

Computational Methods

All atomic structures and energies reported herein were calculated using spin-polarized DFT within the generalized gradient approximation (GGA-PBE)[11] as implemented in the Vienna Ab initio Simulation Package (VASP).[12] To treat the strong on-site 3*d* electron-electron interactions on Fe an additional Hubbard-U was added ($U_{eff} = 4.3$ eV),[13] which is a widely accepted value for the particular material system ($FePO_4$ or $LiFePO_4$), rendering accurate prediction of material properties such as bandgap. The projected augmented wave method[14,15] with a plane-wave basis set (E_{cut} = 450 eV) was employed, and all atoms were fully relaxed until residual forces on constituent atoms became smaller than 1×10^{-2} eV/Å. The pristine $FePO_4$ was modeled using a 24-atom unit cell while the PO_4-deficient structure was created by removing a PO_4 unit from an expanded ($1 \times 2 \times 3$), 144-atom supercell. For Brillouin zone sampling, ($3 \times 4 \times 5$) and ($3 \times 3 \times 1$) k-point meshes in the scheme of Monkhorst-Pack[16] were used for the pristine and PO_4-deficient cases, respectively.

Results and Discussion

As illustrated in Fig. 1a (top right inset), $FePO_4$ has an orthorhombic olivine structure (space group *Pnma*) where each PO_4 unit is connected to 5 FeO_6 units; Fe atoms are located on corner-sharing octahedral sites while P atoms on tetrahedral sites. The predicted lattice constants of $a = 9.97$, $b = 5.91$, and $c = 4.88$ Å are in good agreement with the experimental values of a = 9.7599(8), b = 5.7519(5), and c = 4.7560(4) Å.[17] The slight overestimation of lattice constant is mainly attributed to the well-known tendency of GGA to underestimate the bond strength.

Fig. 1a shows the electron density of states (DOS) projected onto Fe, P, and O atoms of pristine $FePO_4$; the top of the valence band (VB) is dominated by O 2*p* states with a small contribution from Fe 3*d* states, whereas the bottom of the conduction band (CB) is mainly composed of Fe 3*d* states. The predicted gap of 1.75 eV is very close to the experimental value of 1.7 eV.[18] In $FePO_4$, Fe^{3+} is found to have a high-spin d^5 electron configuration,[19] yielding the fully occupied spin-up and empty spin-down states. The magnetic moment is predicted to be 4.3 μ_B (per Fe), in excellent agreement with existing experimental data ($\approx$ 4.15 μ_B);[18] the relatively smaller value compared to the free Fe^{3+} case (= 5 μ_B)[20] is apparently attributed to the hybridization with O 2*p* orbitals. It is also worth pointing out that the distinct overlap between P 3*s*/3*p* and O 2*p* orbitals is far below the Fermi level, implying the relatively stronger interaction of O atoms with P atoms than Fe atoms.

Next, we examined how the deficiency of PO_4 polyanions alters the electronic structure and geometry of $FePO_4$. While neighboring atoms are noticeably displaced, four of the five Fe atoms adjacent to the neutral PO_4 vacancy ($V^0_{PO_4}$) become fivefold coordinated and the rest is fourfold coordinated. The removal of a neutral PO_4 unit leaves three unpaired electrons which tend to localize on adjacent Fe atoms. As presented in Fig. 1b, the projected DOS of the PO_4-deficient structure exhibits two distinct defect states within the bandgap. One defect level (indicated as I) lies just above the VB, and the other (II) is in the middle of the gap. The defect state I shows overlap between spin-up Fe 3*d* and O 2*p* orbitals while spreading over neighboring Fe and O atoms (as demonstrated by the band-decomposed charge density plot in Fig. 1b (top right inset); this suggests the defect level is associated with lattice distortions around $V^0_{PO_4}$. On the other hand, as shown in Fig. 1b (bottom right inset), the excess electrons associated with defect state II seem to be highly localized on three neighboring Fe atoms; this is not surprising considering that Fe 3*d* states dominate the bottom of the CB in $FePO_4$, thus readily accepting excess electrons. Due to such charge localization, the neighboring three Fe atoms (a, b and c) are reduced to Fe^{2+} [Fig. 2a]. The local lattice surrounding $V^0_{PO_4}$ exhibits an outward expansion, and the adjacent P atom is displaced slightly in [010] direction toward $V^0_{PO_4}$; consequently, the P-Fe (I)

*Electrochemical Society Student Member.
**Electrochemical Society Active Member.
zE-mail: gshwang@che.utexas.edu

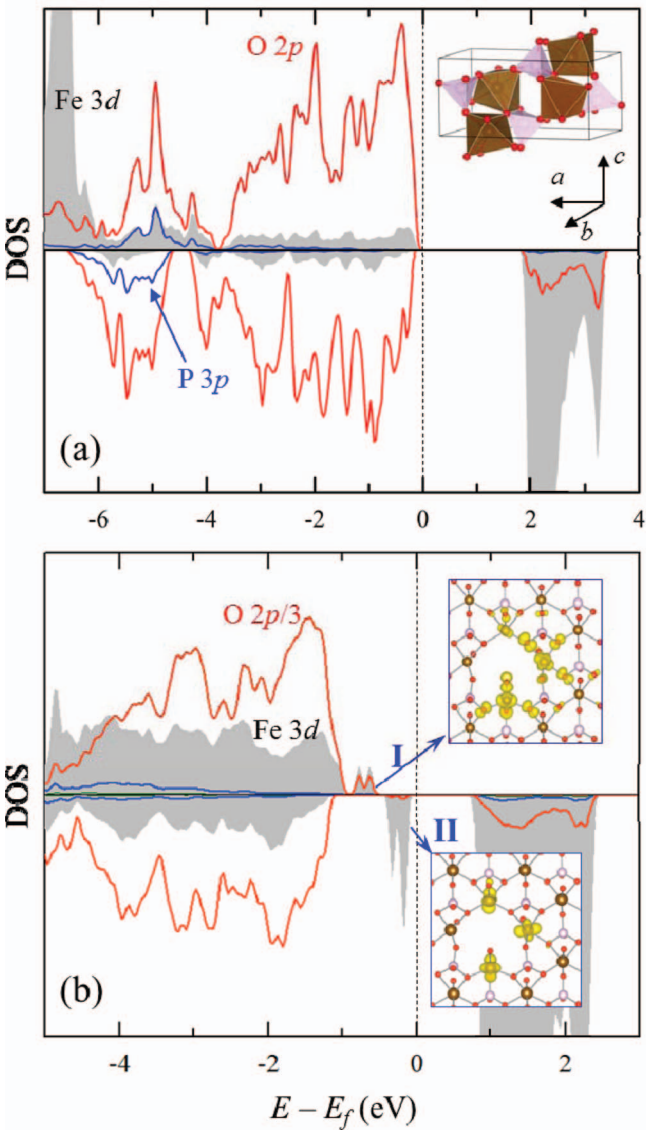

Figure 1. The electron density of states (DOS) projected on Fe, P and O atoms in (a) pristine and (b) PO_4-deficient $FePO_4$; the shaded gray area represents Fe 3*d* states, and the blue and red solid lines indicate P 3*p* and O 2*p* states, respectively [note the intensity of O 2*p* state in (b) is rescaled by 1/3]. The inset in (a) shows a unit cell of pristine $FePO_4$. The band-decomposed charge densities corresponding to defect states I and II are plotted with an isosurface value of 0.005 electron/Å^3 as shown in the top and bottom right insets in (b).

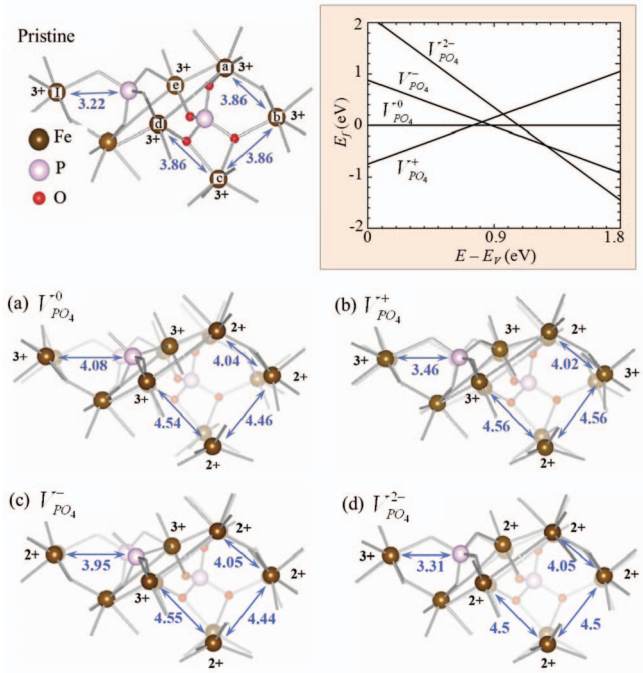

Figure 2. Optimized configurations for pristine (top left) and PO_4-deficient $FePO_4$ in (a) neutral ($V^0_{PO_4}$), (b) positive ($V^+_{PO_4}$), (c) negative ($V^-_{PO_4}$), and (d) doubly negative ($V^{2-}_{PO_4}$) charge states. The charge states for Fe and P atoms near the PO_4 unit/vacancy are labeled in black; the Fe-Fe and P-Fe distances labeled in blue are given in angstrom. (Top right) Variation in the relative formation energy of PO_4-deficient $FePO_4$ in different charge states with respect to $V^0_{PO_4}$ as a function of the Fermi level relative to the valence bend maximum (E_v) for the computed $FePO_4$ bandgap around 1.75 eV.

distance increases from 3.22 Å (in the pristine case) to 4.08 Å. It is worth noting that the $V^0_{PO_4}$-induced lattice distortion appears to be asymmetrical with respect to the (010) plane spanned by Fe (a, c and e) as the Fe (c)-(b) and (c)-(d) distances are different (4.46 and 4.54 Å, respectively). The slight deviation from symmetry is likely attributed to the unequal charge redistribution among the five Fe ions adjacent to $V^0_{PO_4}$, resulting in their differences in charge state and bond environment.

We also looked at the structures and relative stabilities of PO_4-deficient $FePO_4$ in positive ($V^+_{PO_4}$), negative ($V^-_{PO_4}$), and doubly negative ($V^{2-}_{PO_4}$) charge states. For $V^+_{PO_4}$ [Fig. 2b], with an additional hole, one of the three Fe^{2+} ions in $V^0_{PO_4}$ is oxidized to Fe^{3+} (a). The lattice distortion becomes symmetrical as two Fe ions (b and d) locating on the opposite sides of the (010) plane have the same charge state (3+); in addition, we also found the displacement of the adjacent P atom to be much smaller if the lattice distortion was symmetrical. For $V^-_{PO_4}$ [Fig. 2c], the additional electron tends to localize on Fe (I), and the lattice distortion is asymmetrical. For $V^{2-}_{PO_4}$ [Fig. 2d], with additional two electrons, all five Fe^{3+} ions surrounding the PO_4 vacancy are reduced to Fe^{2+}, thus the symmetric configuration is restored, and the P-Fe (I) distance of 3.31 Å is very close to the pristine case (3.22 Å).

Fig. 2 (top right) shows the relative formation energy of PO_4-deficient $FePO_4$ in positive ($V^+_{PO_4}$), negative ($V^-_{PO_4}$), and doubly negative ($V^{2-}_{PO_4}$) charge states with respect to $V^0_{PO_4}$, which is calculated by $E^f(V^q_{PO_4}) = E_{tot}(V^q_{PO_4}) - E_{tot}(V^0_{PO_4}) + q(E_v + \varepsilon_F)$, where E_{tot} is the total energy of the supercell, q is the charge state, E_v is valence band maximum (VBM), and ε_F is the Fermi level. In the periodic approach, a homogeneous background charge is included to maintain the overall charge neutrality of a charged supercell. To account for the electrostatic interaction with the background charge, a monopole correction was made to the total energy of the charged system.[21] For a point-like charge in the 144-atom $FePO_4$ supercell, the monopole correction is estimated to be smaller than 0.1 eV, which is reasonable given the considerably large dielectric constant of 17.5.[22] Our calculation predicts the relative formation energies of $V^+_{PO_4}$, $V^-_{PO_4}$ and $V^{2-}_{PO_4}$ to be −0.77, 0.76 and 1.83 eV at the VBM, respectively. Given the calculated $FePO_4$ bandgap around 1.75 eV, the first donor (+/0) and acceptor (0/−), and the second acceptor levels (−/2−) are predicted to be 0.7, 0.87, and 1.08 eV, respectively. At the midgap ($\varepsilon_F \approx 0.88$ eV), $V^-_{PO_4}$ has the lowest formation energy around −0.15 eV, suggesting that $V^0_{PO_4}$ may easily accommodate an additional electron under the intrinsic condition; considering their small formation energy difference, $V^0_{PO_4}$ and $V^-_{PO_4}$ may coexist in the matrix.

Finally, we looked at how the PO_4 deficiency affects the mechanical properties. Here we only considered the bulk modulus (B) which can be estimated by fitting the Murnaghan equation of state[23] to the corresponding energy versus volume curve. Uniform tensile and

compressive strains were imposed on the pristine and PO_4-deficient ($V^0_{PO_4}$) $FePO_4$ structures to achieve ± 0.66% volume changes.

$$E(V) = E_0 + \left(\frac{BV}{B'}\right)\left[\frac{(V_0/V)^{B'}}{B'-1} + 1\right] - \frac{V_0 B}{B'-1} \quad [1]$$

where E and E_0 refer to the total energies of pristine and PO_4-defficient $FePO_4$ at volume V and V_0 (equilibrium), respectively, and B' is the pressure derivative of the bulk modulus; here, we increased the cut-off energy to 550–600 eV and force tolerance to 0.01 eV/Å to refine energy variations with applied strain. While the predicted B value of 68.1 GPa for pristine $FePO_4$ is in close agreement with previous result (≈ 73.6 GPa),[24] our calculations show a 20% reduction in B (≈ 53.2 GPa) with only 4.2 at.% $V^0_{PO_4}$ in the $FePO_4$ matrix. We anticipate such significant softening effect to have substantial impacts on Li diffusion in PO_4-deficient $FePO_4$, which is under investigation. As suggested by previous theoretical study, Li diffusion can be substantially enhanced in the strained (tensile) $LiFePO_4$ lattice due to the excess space allowing Li migration; similar effects may be expected from the softened lattice.[25]

Conclusions

DFT+U calculations were performed to investigate the structure and properties of PO_4-deficient $FePO_4$ at various charge states ($V^q_{PO_4}$, $-2 \le q \le +1$). The unpaired electrons associated $V^q_{PO_4}$ tend to localize on adjacent undercoordinated Fe atoms, which undergo outward displacements. The $V^q_{PO_4}$ -induced lattice distortions are found to be sensitive to q. At the midgap, $V^-_{PO_4}$ has the lowest formation energy (0.15 eV lower than that of $V^0_{PO_4}$), but given the small energy difference, $V^0_{PO_4}$ and $V^-_{PO_4}$ are likely to coexist. We also find that PO_4-deficiency can effectively soften the matrix as the bulk modulus (≈ 53.2 GPa) is reduced by 20% from the pristine case. The more flexible PO_4-deficient $FePO_4$ may thereby lower the diffusion barrier, contributing to enhanced Li mobility. Our fundamental findings shed light on a new approach to defect engineering toward the design of high performance $LiFePO_4$ cathode.

Acknowledgment

This work was partially supported by the Welch Foundation (F-1535) and the National Science Foundation (DMR-1122603). We would like to thank the Texas Advanced Computing Center for use of their computing resources. Yu-Hao Tsai and Chia-Yun Chou contributed equally to the manuscript.

References

1. M. Takahashi, S. Tobishima, K. Takei, and Y. Sakurai, *J. Power. Sources*, **97-98**, 508 (2001).
2. Y. Wang, P. He, and H. Zhou, *Energy Environ. Sci.*, **4**, 805 (2011).
3. L.-X. Yuan, Z.-H. Wang, W.-X. Zhang, X.-L. Hu, J.-T. Chen, Y.-H. Huang, and J. B. Goodenough, *Energy Environ. Sci.*, **4**, 269 (2011).
4. J. Li, W. Yao, S. Martin, and D. Vaknin, *Solid State Ionics*, **179**, 2016 (2008).
5. S. Chung, J. Bloking, and Y. Chiang, *Nat. Mater.*, **1**, 123 (2002).
6. M. Park, X. Zhang, M. Chung, G. B. Less, and A. M. Sastry, *J. Power Sources*, **195**, 7904 (2010).
7. M. S. Islam, D. J. Driscoll, C. A. J. Fisher, and P. R. Slater, *Chem. Mater.*, **17**, 5085 (2005).
8. G. K. P. Dathar, D. Sheppard, K. J. Stevenson, and G. Henkelman, *Chem. Mater.*, **23**, 4032 (2011).
9. K. Hoang and M. Johannes, *Chem. Mater.*, **23**, 3003 (2011).
10. K. H. Song, S. Y. Han, H. S. Nam, E. Y. Bang, S. J. Oh, I. J. Baek, S. Y. Kim, and K. S. Han, U.S. Patent Application No. 12/685,749, Publication No. 20100183924 (2010).
11. J. P. Perdew, K. Burke, and M. Ernzerhof, *Phys. Rev. Lett.*, **77**, 3865 (1996); J. P. Perdew, K. Burke, and M. Ernzerhof, *Phys. Rev. Lett.*, **78**, 1396 (1997).
12. G. Kresse and J. Furthmüller, *Comput. Mat. Sci.*, **6**, 15 (1996); G. Kresse and J. Furthmüller, *Phys. Rev. B*, **54**, 11169 (1996).
13. F. Zhou, M. Cococcioni, C. A. Marianetti, D. Morgan, and G. Ceder, *Phys. Rev. B.*, **70**, 235121 (2004).
14. P. E. Blochl, *Phys. Rev. B*, **50**, 17953 (1994).
15. G. Kresse and D. Joubert, *Phys. Rev. B*, **59**, 1758 (1999).
16. H. J. Monkhorst and J. D. Pack, *Phys. Rev. B*, **13**, 5188 (1976).
17. G. Rousse, J. Rodriguez-Carvajal, S. Patoux, and C. Masquelier, *Chem. Mater.*, **15**, 4082 (2003).
18. J. Gou, *Proc SPIE*, **6650**, 66500F (2007).
19. F. Zhou, K. Kang, T. Maxish, G. Ceder, and D. Morgan, *Solid State Commun.*, **132**, 181 (2004).
20. Y.-N. Xu, W. Y. Ching, and Y.-M. Chiang, *J. Appl. Phys.*, **95**, 6583 (2004).
21. G. Makov and M. C. Payne, *Phys. Rev. B*, **51**, 4014 (1995).
22. C. Kuss, G. Liang, and S. B. Schougaard, *J. Mater. Chem.*, **22**, 24889 (2012).
23. F. D. Murbaghan, *Proc. Natl. Acad. Sci.*, **30**, 244 (1994).
24. T. Maxish and G. Ceder, *Phys. Rev. B*, **73**, 174112 (2006).
25. J. Lee, S. J. Pennycook, and S. T. Pantelides, *Appl. Phys. Lett.*, **101**, 033901 (2012).